We thank the anonymous reviewer for the comments on our manuscript. The comments and suggestions are greatly appreciated. All the comments have been addressed and we believe that the revisions based on these comments have improved the quality of our manuscript. Below please find our responses to the comments one by one and the corresponding revisions made to the manuscript. The original comments are in italics. The revised parts of the manuscript are in blue here and can be followed in the revised manuscript with track changes with line numbers indicated.

Responses to reviewer 1:

Reviewer: 1

Comments:

Secondary organic aerosol (SOA) may contribute significantly to cloud condensation nuclei (CCN), yet relevant research of explicit simulation remains relatively limited. While existing SOA modeling studies predominantly concentrate on mass concentration, this work specifically investigates the CCN activity of SOA, thereby advancing our understanding of SOA's role in CCN formation. My specific comments are as follows:

(1) Although the paper is titled " Explicit simulation of chemical composition, size distribution and cloud condensation nuclei of secondary organic aerosol from α-pinene ozonolysis", it only provides detailed descriptions for the size distribution and CCN simulations, with inadequate description on the chemical composition of SOA. For instance, the number of species involved in gas-particle partitioning in the model remains unspecified. Furthermore, no information is provided regarding whether the gaseous concentrations of these species were characterized with experimental observations or have undergone laboratory validation. The authors should provide a list of substances involved in gas-particle transformation in supplement file.

Response:

Accepted. In our experiments SOA chemical composition was measured by AMS (e.g. O:C and H:C ratios). Although PyCHAM can simulate the gas–particle partitioning of all species involved in the chemical mechanism (MCM+PRAM) and calculate their concentrations across particle-phase size bins, we lack direct molecular-level information on individual compounds in the particle-phase. For this reason, the main text focuses on discussing the elemental composition (ratios of different elements) of SOA.

Gas-phase species participating in gas-particle partitioning, mainly oxygenated organic molecules (OOMs), were measured using a nitrate-CIMS.

In the revised manuscript, we have clearly described the measurements of organic compounds participating in gas-particle partitioning as follows (line 139-141).

"Gas-phase oxygenated organic molecules (OOMs) participating in gas-particle partitioning, including HOMs, were measured using a chemical ionization atmospheric pressure interface time-of-flight mass spectrometer (CIMS, Tofwerk AG/Aerodyne Research, Inc.) with nitrate (NO_3^-) as the reagent ion (NO_3^--CIMS)."

We have also included in the Supplement the chemical formulas of all organic species (including HOMs) produced by MCM and PRAM mechanisms (Table S1), and the corresponding text were added in the main manuscript in line 234-235.

"The detailed chemical species formulas produced by MCM and PRAM mechanisms are shown in Table S1."

Table S1 is shown below:

Chemical species in MCM or PRAM			
CH3O2	C9PAN2	C721PAN	C18H26O4
CH3O	C85CO3H	C721CO3H	C88O2
CH3NO3	C85OOH	NORPINIC	C718CO3
HCHO	C86OOH	C721OOH	C87O2
CH3O2NO2	C511OOH	C722OOH	NC826O2
CH3OOH	C7PAN3	C44OOH	C18H27O6NO3
CH3OH	C235C6CO3H	C811NO3	C20H30O8
CO23C4CHO	CO235C6OOH	C516O	C20H31O6NO3
BIACETO2	APINBO	C516OOH	C19H28O9
CH3CO3	APINBNO3	C10H15O2O2	C19H29O6NO3
HCOCH2CO3	APINBOOH	LIMOOA	C18H26O9
CO23C4CO3	APINBCO	LIMALAO2	C18H27O7NO3
C5PAN9	NAPINAO2	LIMALBO2	C20H30O9
CO23C4CO3H	NAPINBO2	C10H17O3O2	C20H31O7NO3
CO23C3CHO	NAPINAO	BPINENE	C19H28O10
HCOCH2CHO	NAPINAOOH	LIMONENE	C19H29O7NO3
HCOCH2O2	NAPINBO	CARENE	C18H26O10
C3PAN2	NC101CO	C10H15O4O2	C18H27O8NO3
HCOCH2CO3H	NAPINBOOH	C10H15O3O2	C20H30O10
HCOCH2CO2H	NC101O2	C10H15O5O2	C20H31O8NO3
GLYOX	NC101O	C10H15O6O2	C19H28O11
BIACETO	NC102O2	C10H15O7O2	C19H29O8NO3
BIACETOOH	NC102O	C10H15O8O2	C18H26O11
BIACETOH	NC71O2	C10H15O9O2	C18H27O9NO3
HOCH2CO3	NC71O	C10H15O10O2	C20H30O11
HOCH2CHO	NC71CO	C10H15O11O2	C20H31O9NO3
PHAN	NC101OOH	C10H15O12O2	C19H28O12
HOCH2CO3H	NC102OOH	C10H15O2O	C19H29O9NO3
HOCH2CO2H	NC71OOH	C10H15O3O	C18H26O12
ACETOL	NC72O2	C10H15O4O	C18H27O10NO3
MGLYOX	NC72O	C10H15O5O	C20H30O12
CH3COCH2O2	NC61CO3	C10H15O6O	C20H31O10NO3
CH3COCH2O	NC72OOH	C10H15O7O	C19H28O13
HCOCO	NC6PAN1	C10H15O8O	C19H29O10NO3

HCOCO3	NC61CO3H	C10H15O9O	C18H26O13
HCOCO3H	APINCO	C10H15O10O	C18H27O11NO3
HCOCO2H	APINCNO3	C10H15O11O	C20H30O13
HMVKAO2	C720O2	C10H15O12O	C20H31O11NO3
HMVKAO	APINCOOH	C10H14O3	C19H28O14
HMVKANO3	APINCOH	C10H14O4	C19H29O11NO3
HMVKAOOH	HCC7CO	C10H14O5	C18H26O14
HO12CO3C4	C720O	C10H14O6	C18H27O12NO3
CO2H3CHO	C720NO3	C10H14O7	C20H30O14
CO2H3CO3	C720OOH	C10H14O8	C20H31O12NO3
C4PAN6	C720OH	C10H14O9	C19H28O15
CO2H3CO3H	C719O2	C10H14O10	C19H29O12NO3
PAN	C719O	C10H14O11	C18H26O15
CH3CO3H	C719NO3	C10H14O12	C18H27O13NO3
CH3CO2H	C719OOH	C10H14O13	C20H30O15
HCOCH2O	C719OH	C10H15O2NO3	C20H31O13NO3
HCOCH2OOH	APINOOA	C10H15O3NO3	C19H28O16
CH3COCH3	APINOOB	C10H15O4NO3	C19H29O13NO3
HYPERACET	C107O2	C10H15O5NO3	C18H26O16
CHOC3COCO3	C109O2	C10H15O6NO3	C18H27O14NO3
CHOC3COO2	C107O	C10H15O7NO3	C20H30O16
CHOC3COO	C108O2	C10H15O8NO3	C20H31O14NO3
CHOC3COPAN	C108O	C10H15O9NO3	C19H28O17
CHOC3COOOH	C108NO3	C10H15O10NO3	C19H29O14NO3
C413COOOH	C717O2	C10H15O11NO3	C18H26O17
C4CODIAL	C717O	C10H15O12NO3	C18H27O15NO3
C312COCO3	C717NO3	C10H16O4iso1	C20H30O17
CHOCOCH2O2	C107OOH	C10H16O5iso1	C20H31O15NO3
CHOCOCH2O	C107OH	C10H16O6iso1	C19H28O18
C312COPAN	C108OOH	C10H16O7iso1	C19H29O15NO3
C312COCO3H	C108OH	C10H16O8iso1	C18H26O18
ALCOCH2OOH	C717OOH	C10H16O9iso1	C18H27O16NO3
C33CO	C717OH	C10H16O10	C10H16O3
H1CO23CHO	C109O	C10H16O11	C10H17O5O2
APINENE	C89CO3	C10H16O12	C10H17O4O2
APINAO2	C920CO3	C10H16O13	C10H17O6O2
APINBO2	C109OOH	C10H16O14	C10H17O7O2

APINCO2	C109OH	C20H30O5	C10H17O8O2
APINAO	C109CO	C20H30O6	C10H17O3O
APINANO3	C920O2	C20H30O7	C10H17O4O
PINAL	C920O	C923CO3	C10H17O5O
APINAOOH	C921O2	LIMAO2	C10H17O6O
APINBOH	C921O	LIMCO2	C10H17O7O
C96O2	C922O2	LIMALO2	C10H16O4iso2
C96CO3	C922O	LIMBO2	C10H16O5iso2
PINALO2	C621O2	C20H31O4NO3	C10H16O6iso2
C96O	C621O	BPINAO2	C10H16O7iso2
C96NO3	H1C23C4CHO	BPINBO2	C10H16O8iso2
C97O2	H1C23C4O2	BPINCO2	C10H16O9iso2
C97O	H1C23C4CO3	C918CO3	C10H17O3NO3
C98O2	H1C23C4O	C20H31O5NO3	C10H17O4NO3
C98O	H1C23C4PAN	NLIMO2	C10H17O5NO3
C98NO3	HC23C4CO3H	NLIMALO2	C10H17O6NO3
C614O2	H1C23C4OOH	NC91CO3	C10H17O7NO3
C614O	C920PAN	NBPINAO2	C10H17O8NO3
C614NO3	C920CO3H	NBPINBO2	C10H18O5
PINALO	HOPINONIC	C19H28O5	C10H18O6
PINALNO3	C920OOH	C19H28O6	C10H18O7
C106O2	C921OOH	C19H28O7	C10H18O8
C106O	C922OOH	C19H28O8	C10H18O9
C106NO3	C621OOH	C923O2	C10H18O10
C716O2	APINBOO	C924O2	C20H34O6
C716O	C89CO2	C816CO3	C20H34O7
CO13C4CHO	C89O2	NORLIMO2	C20H34O8
C10PAN2	C89O	LMKAO2	C20H35O5NO3
PERPINONIC	C89NO3	LMKBO2	C20H35O6NO3
PINONIC	C810O2	C926O2	C19H32O6
C96OOH	C810O	C817CO3	C19H32O7
C96OH	C810NO3	LMLKAO2	C19H32O8
NORPINAL	C514O2	LMLKBO2	C19H32O9
C97OOH	C514O	C823CO3	C19H33O6NO3
C97OH	C514NO3	C925O2	C18H30O6
C98OOH	C89PAN	NOPINAO2	C18H30O7
C98OH	C89CO3H	NOPINBO2	C18H30O8

C614OOH	C89CO2H	NOPINCO2	C18H30O9
C614OH	C89OOH	NOPINDO2	C18H30O5
C614CO	C89OH	C918O2	C18H31O7NO3
PINALOOH	C810OOH	C9DCO2	C20H34O9
PINALOH	C810OH	C915O2	C20H35O7NO3
C106OOH	C514OOH	C917O2	C19H32O10
C106OH	C514OH	C919O2	C19H33O7NO3
C716OOH	C811CO3	C914O2	C18H30O10
C716OH	C811O2	C916O2	C18H31O8NO3
CO235C6CHO	C811O	C88CO3	C20H34O10
H3C25C6O2	C812O2	C87CO3	C20H35O8NO3
H3C25C6CO3	C812O	C822CO3	C19H32O11
H3C25C6O	C813O2	NLMKAO2	C19H33O8NO3
H3C2C4CO3	C813O	C19H29O5NO3	C18H30O11
H3C2C4PAN	C813NO3	C18H26O5	C18H31O9NO3
H3C2C4CO3H	C516O2	C18H26O6	C20H34O11
H3C2C4CO2H	C811CO3H	C18H26O7	C20H35O9NO3
H3C25C6PAN	PINIC	C729CO3	C19H32O12
H3C25C5CHO	C811PAN	C816O2	C19H33O9NO3
H3C25CCO3H	C811OOH	C817O2	C18H30O12
H3C25CCO2H	C811OH	C826O2	C18H31O10NO3
H3C25C6OOH	C721CHO	C822O2	C20H34O12
H3C25C6OH	C812OOH	C818O2	C20H35O10NO3
C85O2	C812OH	C823O2	C19H32O13
C85CO3	C813OOH	C819O2	C19H33O10NO3
C85O	C813OH	C727CO3	C18H30O13
C86O2	CO13C3CO2H	C731CO3	C18H31O11NO3
C86O	C721O2	C824O2	C20H34O13
C511O2	C721CO3	C820O2	C20H35O11NO3
C511O	C721O	C18H26O8	C19H32O14
CO235C5CHO	C722O2	C825O2	C19H33O11NO3
CO235C6CO3	C722O	C821O2	C18H30O14
CO235C6O2	C44O2	C732CO3	C18H31O12NO3
CO235C6O	C44O	C8BCO2	C10H18O4

(2) Accurate simulation of CCN critically depends on both number concentration and particle size distribution. Notably, the authors employed two distinct methods for number concentration: when modeling CCN, they utilized

observation-derived fitting results, whereas for SOA mass simulation, they adopted a nucleation scheme based on C20H30O17 molecule. Why were these two methods applied separately? Are the simulation results from these two approaches comparable?

Response:

When modeling SOA mass concentration and chemical composition, we used nucleation scheme. In the current version of PyCHAM, the nucleation process can only be constrained using three parameters that determine the initial growth of particle number concentration. However, the particle size distribution (PSD) during the early nucleation stage cannot be set in nucleation scheme. As a result, the simulated PSD exhibits a clear bias in peak position relative to the observations. Figure R1 illustrates the PSD at reaction time of 2 h. Because the accuracy of CCN number concentration depends on both the SOA size distribution and the hygroscopicity parameter (κ), any bias in the PSD directly affects the CCN simulation. To improve the representation of early growth, we constrained the initial PSD using the SMPS measurements and assuming a seed aerosol, i.e. using seed scheme. The PSD at reaction time hour 2 is shown below (Fig. R2); this approach performs better than the nucleation scheme in simulating PSD. However, since this approach requires specifying an explicit seed species, we selected $C_{20}H_{30}O_{17}$—an organic molecule with sufficiently low vapor pressure—as the seed. In this case, the simulated SOA mass and O:C ratio are thus influenced by the assumed seed composition, ultimately increasing the discrepancy with observations (Fig. R3). Consequently, the overall performance on chemical composition is worse than the nucleation scheme.

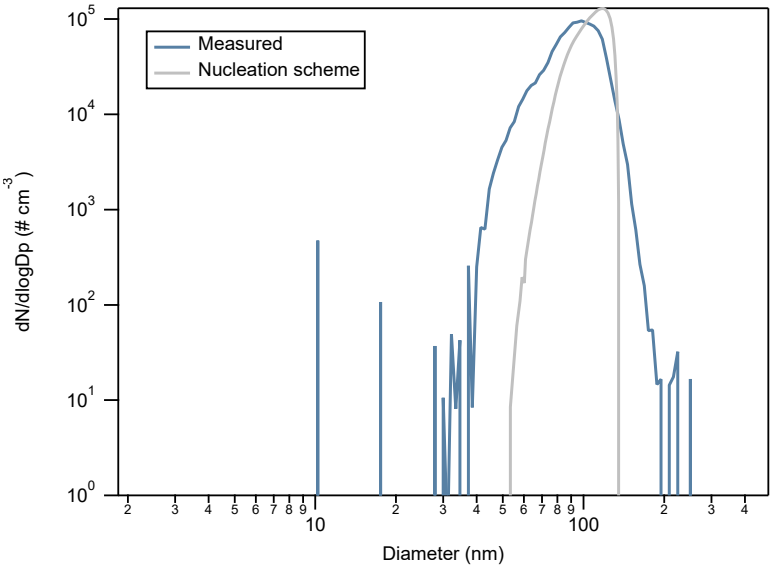

Fig. R1: The measured and nucleation scheme-simulated particle size distribution (PSD) at the reaction time of 2 h.

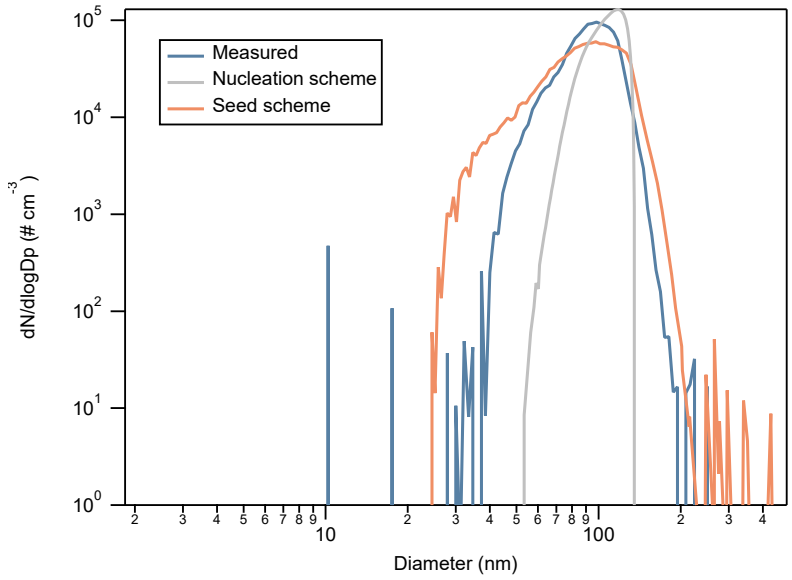

Fig. R2: Same as Fig. R1, with the addition of the PSD simulated by the seed scheme.

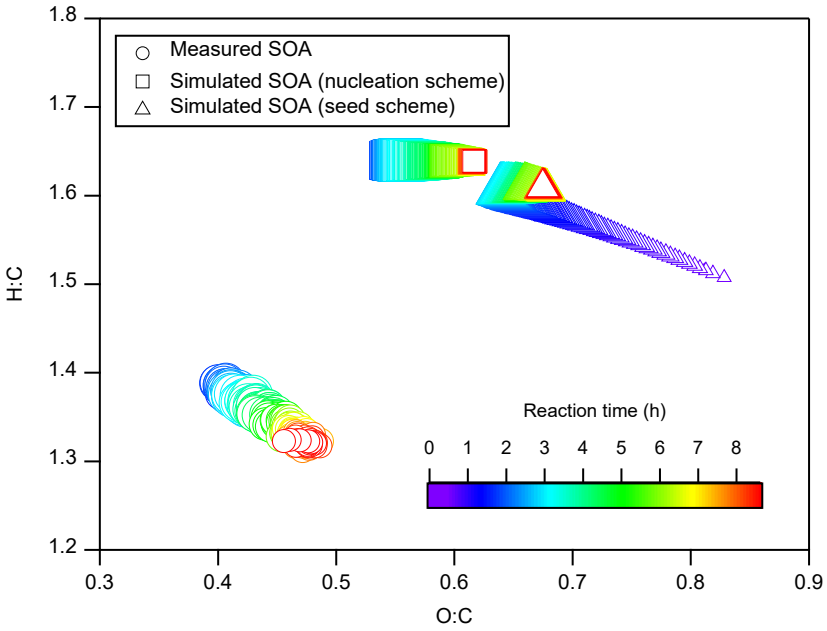

Fig. R3: O:C and H:C distributions of SOA measured experimentally and simulated using the two schemes (nucleation and seed).

To obtain accurate CCN predictions, bulk κ of SOA was calculated from the chemical composition derived using the nucleation scheme, and was subsequently combined with the PSD from the seed scheme to compute CCN. Admittedly, this hybrid approach may lack coherence and general applicability. To assess how each scheme influences CCN results, we first applied the nucleation scheme consistently for both SOA κ and CCN simulations (Fig. R4), and compared the resulting CCN with those presented in the main text (Fig. 7). This isolates the influence of PSD on CCN. The results indicate that the PSD of both schemes obtain similar CCN number concentrations, which are close to observations at supersaturation (SS) = 0.55% and 0.73%. Under the nucleation scheme, CCN at SS = 0.37% is slightly overestimated, and CCN at SS = 0.19% is initially higher than observations but gradually decreases toward zero.

Next, we applied the seed scheme consistently for both SOA κ (Fig. R5) and CCN simulations (Fig. R6) and compared these CCN values with those in the original manuscript. This isolates the influence of κ on CCN. Both schemes demonstrate similar CCN prediction performance across four SS, though CCN simulated by the seed scheme was slightly

lower than that of the combined scheme as a result of lower simulated κ (Fig. R5).

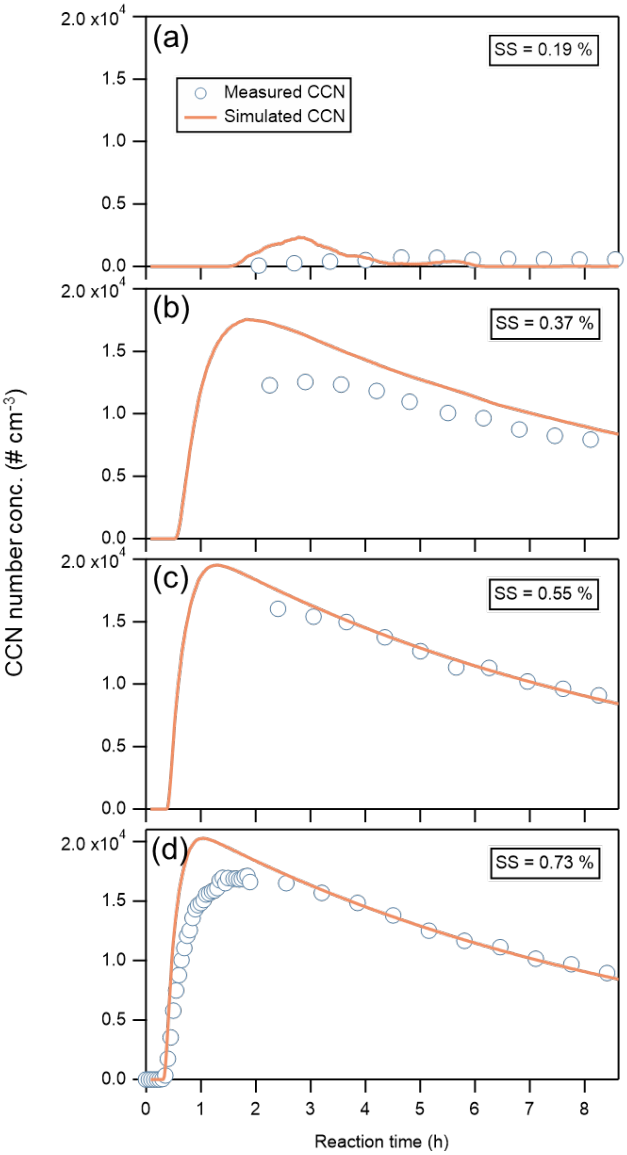

Fig. R4: CCN number concentrations (# cm^{-3}) measured experimentally and simulated using κ and PSD from nucleation scheme.

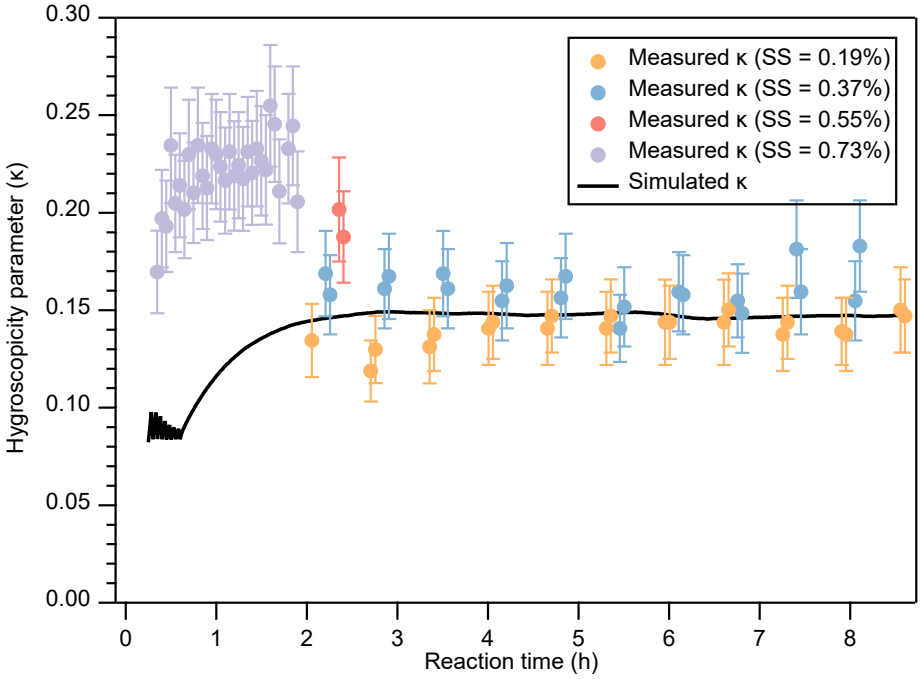

Fig. R5: Measured and simulated (using the seed scheme) SOA κ.

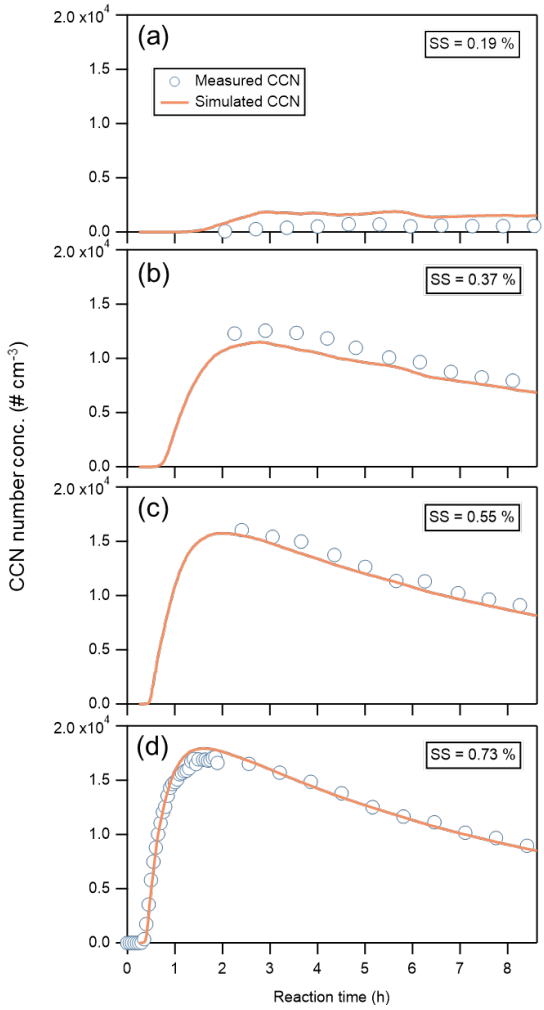

Fig. R6: Same as Fig. R4, but for CCN simulated by κ and PSD from seed scheme.

Overall, if the nucleation scheme is applied alone, the simulated PSD performs worse than that obtained with the combined approach, resulting in larger bias of CCN concentrations at the two lower SS. In contrast, applying the seed

scheme alone leads to worse simulations of initial SOA mass concentration, chemical composition, and κ due to the assumed composition of seed species. However, because the PSD remains relatively accurate, the resulting CCN concentrations are similar to those from the combined approach. Therefore, in this study we adopted the combined approach, which reconciles the simulations of both chemical composition and PSD while minimizing bias in CCN predictions.

We have added the description about the influence of two independent schemes on CCN predictions in Sect. 3.4 (line 452-465).

"**3.4 Discussion of the influence of individual schemes (nucleation vs. seed) on CCN predictions**

To demonstrate the rationale for the combined approach - using κ from the nucleation scheme together with PSD from the seed scheme - a detailed analysis of the effect of applying each scheme independently on the CCN simulations is implemented.

As shown in Fig. S21, CCN calculated using the κ by the nucleation scheme (Fig. 6) and PSD by the same scheme (Fig. S4) at SS = 0.55% and 0.73% were comparable to those from the combined-scheme approach. However, at SS = 0.37%, CCN was moderately overestimated, and at SS = 0.19% the predicted CCN was initially higher than the measurements and then decreased toward zero. In contrast, CCN calculated using the κ from the seed scheme (Fig. S22) combined with its PSD (Fig. 5) produced lower CCN across all four SS (Fig. S23), leading to a worse performance than that of the combined-scheme approach.

Overall, if the nucleation scheme was applied alone, the simulated PSD performed worse than that obtained with the combined approach, resulting in deviations of CCN concentrations at the two lower SS. In contrast, applying the seed scheme alone led to worse simulations of initial SOA mass concentration, chemical composition, and κ due to the assumed composition of seed species. However, because the PSD remained relatively accurate, the resulting CCN concentrations were similar to those from the combined approach."

Figure S21-23 in the Supplement correspond to Fig. R4-6 here.

(3) Line 116: Please specify the exact model of the DMA in the SMPS. Also, provide the specific model of the AMS, and similarly, specify the models of other equipment used.

Response:

Accepted. We have now specified the instrument models for the DMA, AMS, and CCN measurements in the revised manuscript as follows (line 122-124).

"A scanning mobility particle sizer (SMPS, TSI DMA3081/TSI CPC3785) measured SOA mass and number concentrations and size distributions over the range 9.82–429.4 nm. A cloud condensation nuclei counter (CCN100, Droplet Measurement Technique, USA) measured CCN…"

And line 134-136:

"A high-resolution time-of-flight aerosol mass spectrometer (HR-ToF-AMS, Aerodyne Research Inc., DeCarlo et al., 2006) provided SOA chemical composition data, including O:C and H:C elemental ratios."

(4) Line 119: The authors state that "The SS calibration and κ parameter calculations followed Zhang et al. (2023)," but later in the results section, it is mentioned that κ was measured. The authors should explain how κ was measured in

the experimental section.

Response:

We apologize for the ambiguity. The measured κ are determined using Scanning Mobility CCN Analysis (SMCA) method (Moore et al., 2010). The detailed procedure is referred to our previous studies (Zhao et al., 2015, 2016). Briefly, for each of the four SS, CCN number concentration and total particle number concentration (CN) in each SMPS size bin are measured in parallel by coupling a DMA with a CCN counter and CPC. Particles pass through the DMA and the outgoing air is split into two paths connecting to the CCN counter and CPC. For each particle size, the CN and CCN concentrations are used to calculate the activation fraction (CCN/CN). Then, CCN/CN is fitted with Gaussian error function and the critical activation dry diameter (D_{crit}) at the set SS is the turning point of this function. Then κ parameter at four SS is derived from κ–Köhler equation given different SS and corresponding D_{crit} (Petters and Kreidenweis, 2007). These κ values are what we refer to as "measured κ" in the main text.

In contrast, the simulated κ values are calculated directly from the modeled SOA molecular concentrations, vapor pressures, density, dry diameter, temperature, and surface tension (Kreidenweis et al., 2005). Therefore, the simulated κ does not depend on SS, unlike the observation-derived κ values.

We have added a detailed description of the derivation of the measured κ values in Section 2.1 as follows to clarify this point (line 125-134).

"Based on parallel measurements of CCN and total particle number (cloud nuclei; CN) for each size bin in a continuous flow, the critical activation particle size (D_{crit}) at each SS was determined using the Scanning Mobility CCN Analysis (SMCA) method (Moore et al., 2010; Zhao et al., 2015a, 2016). Briefly, CN and CCN concentrations for each size bin were used to calculate the CCN activation fraction (CCN/CN). Before computing CCN/CN, the measured CCN and CN concentrations were corrected for multiple charged particles. Then, CCN/CN for each charge class was then fitted using a Gaussian error function, and the turning point of this function was taken as D_{crit} at the specific SS. For each SS, at least three full scans were performed, and the resulting D_{crit} were averaged. The SS calibration followed Zhao et al. (2016) and Zhang et al. (2023). Then κ parameter at four SS was derived from κ–Köhler equation given different SS and corresponding D_{crit} (Petters and Kreidenweis, 2007). The error bars for κ were estimated from the standard deviation of D_{crit} across three duplicate scans."

(5) Line 140: Please provide the specific formula used to calculate ki,j, as well as the range and basis for the values of γ and α in this study.

Response:

Accepted. We have added the explicit expression for the mass-transfer coefficient $k_{i,j}$ in the main text (Zaveri et al., 2008). Because no well-established data of activity coefficient γ were available for our experimental conditions, we only simulated the idealized conditions. Non-ideality was neglected, and all activity coefficient γ were set to 1. In our simulations, the accommodation coefficients α for all species were assumed to be 1. These parameter choices have now been clearly stated in the revised manuscript as follows (line 158-166).

"mass accommodation coefficient (α_i) of individual component:

$$k_{i,j} = 4\pi\overline{R_{p,j}}D_{g,i}N_j f\left(Kn_{i,j}, \alpha_i\right), \quad (3)$$

where $\overline{R_{p,j}}$ (cm) is mean wet radius of particles in bin j; $D_{g,i}$ (cm^2 s^{-1}) is gas diffusivity of species i; N_j (cm^{-3}) is

the number concentration of particles in bin j; α_i means the chance that component i can stick to a particle surface when collision happens. In our simulation, α_i for all components were set to 1. And $f(Kn_{i,j}, \alpha_i)$ is the transition regime correction factor to the Maxwellian flux as a function of the Knudsen Number:

$$f(Kn_{i,j}, \alpha_i) = \frac{0.75\alpha_i\,(1 + Kn_{i,j})}{Kn_{i,j}\,(1+ Kn_{i,j}) + 0.283\alpha_i Kn_{i,j} + 0.75\alpha_i}, (4)$$

$$Kn_{i,j} = \frac{\lambda_i}{R_{p,j}}, \quad (5)$$

where λ_i is the mean free path."

And line 155-156:

"Because no well-established data of γ were available for our experimental conditions, we only simulated the idealized conditions (i.e. γ for all components were set to 1)."

(6) Line 165: The authors mention that the aerosol particle size was divided into 128 bins, but later state that it was divided into 106 bins. This inconsistency should be clarified, and the aerosol bin division should be explained in detail in the methods section.

Response:

Accepted. We apologize for the ambiguity. We used 128 size bins in the nucleation scheme, following the sensitivity analysis of O'Meara et al. (2021), who recommends using 128 bins when accurate representation of the PSD is important. In this configuration, the particle size range is set to 1.8–500 nm, with an initial logarithmic bin width of 0.019 nm. Although the upper bound is 500 nm, the simulated $dN/dlogD_p$ is distributed within 9.2–146.2 nm (with values beyond this range being zero).

In the seed-based scheme we used the 106 size bins because the size distribution was constrained by SMPS measurement, which has 106 size bins. The size range is 9.82–429.4 nm, and the average initial logarithmic bin width is approximately 0.016 nm, similar to the bin width in the nucleation scheme. The simulated $dN/dlogD_p$ is mostly distributed within 12.0–215.6 nm (accounting for 99.9% of the total), which is close to that of the nucleation scheme (9.2–146.2 nm).

We have clarified the rationale for choosing 128 or 106 size bins in the revised manuscript as follows (line 196-198).

"As recommended by O'Meara et al. (2021) that a more detailed 128 size bins should be adopted when the number PSD is important, we set the bin number to 128 and employed the full-moving approach to simulate size evolution."

And line 206-208:

"The lower and upper boundaries and mean radii of each size bin and bin number were set according to SMPS (9.82-429.4 nm size range and 106 size bins)."

(7) Lines 196-198: The authors compare measured and simulated values of α-pinene to indicate the capability of PyCHAM with the MCM + PRAM mechanism to describe the gas-phase chemistry of α-pinene ozonolysis. To validate the model's performance in simulating the MCM gas-phase reactions after incorporating the HOMs module, comparing only the reactants is insufficient. It is recommended to also compare the temporal evolution of other major product concentrations, particularly the simulation performance for HOMs.

Response:

Accepted. In the revised version, we further compared the temporal evolution of gas-phase HOMs during the initial 10 min of reaction, including monomers ($C_{10}H_{15}O_8$, $C_{10}H_{14}O_{11}$, $C_{10}H_{16}O_{11}$) and dimers ($C_{20}H_{30}O_{10}$, $C_{20}H_{30}O_{12}$, $C_{20}H_{30}O_{15}$). The model generally well simulated the temporal trend of HOMs, although there are some biases in the absolute concentrations (Fig. R7). Together, these results indicate that the gas-phase chemistry of α-pinene ozonolysis in this study is reasonable.

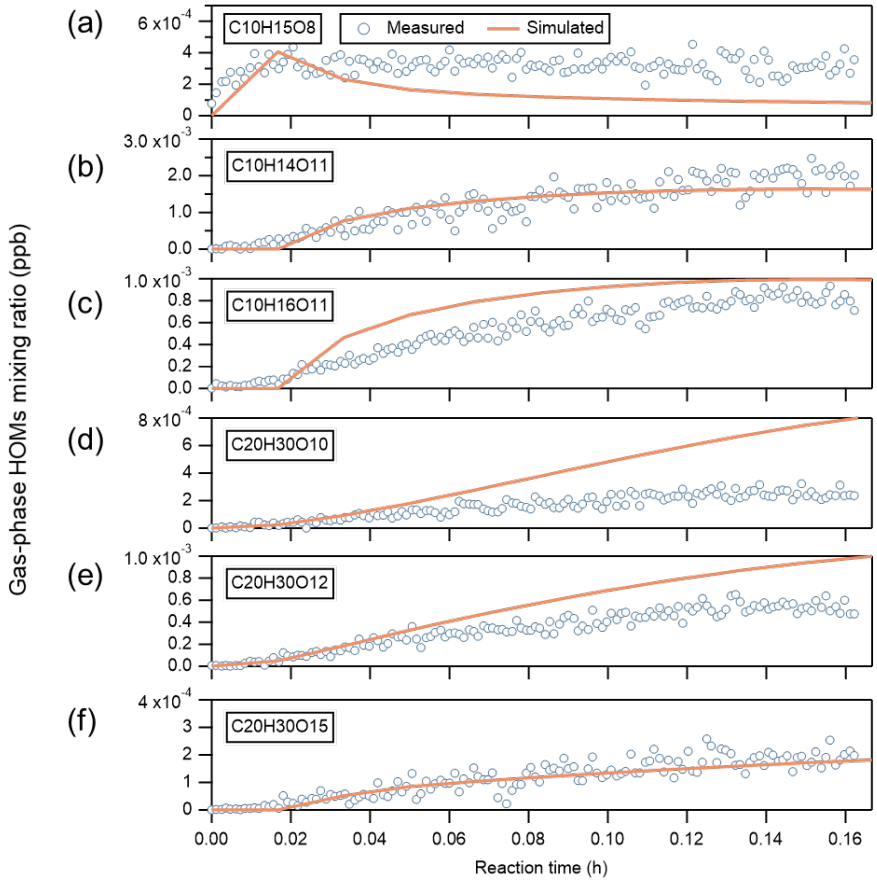

Fig. R7: Measured and simulated time evolution of gas-phase HOMs mixing ratio (ppb) during the initial 10 min of reaction.

We have added the discussion on the gas-phase products HOMs in the main text (line 232-234).

"and the temporal trends of gas-phase products HOMs (Fig. S8) are well captured, though there are some biases in the absolute concentrations, indicating the capability to describe gas-phase chemistry of α-pinene ozonolysis by PyCHAM with MCM and PRAM mechanisms."

Figure S8 in the main text corresponds to Fig. R7 here.

(8) The authors attribute the overestimation of simulated O/C and H/C ratios to the lack of consideration of particle-phase reactions in the model. However, in Figure S6, the simulated HOMs are generally higher than the measured values, especially for ions with m/z above 400. Yet, the total SOA mass concentration is simulated well, implying that the simulation underestimates other components while overestimating HOMs. Clearly, the overestimation of HOMs would lead to higher O/C ratios. Additionally, the authors should analyze the reasons for the overestimation of HOMs in the simulation compared to observations (Figure S6).

Response:

In the original manuscript, we compared the simulated and observed gas-phase HOMs only after normalizing both spectra to their respective maximum signal. We have compared the simulated and observed volume-concentration mass spectra of gas-phase HOMs (Fig. R8). Although the simulated total concentration of gas-phase HOMs during the first 5 min of the experiment (0.011 ppb) is slightly underestimated compared to the measurement (0.014 ppb), the results indicate that the simulation reproduces the observed HOMs species (m/z) reasonably well. Specifically, the concentration levels of dimers are captured closely, while those of monomers are underestimated, particularly at m/z < 300. Our spectra pattern is similar to the findings of Roldin et al. (2019), especially for dimers, who also showed a slight underestimation of monomers. Furthermore, the fractions of HOMs monomers and dimers are also well captured (Fig. R9). These findings together with Fig. R7 suggest that the gas-phase chemical mechanism employed in the model is generally reasonable.

While SOA mass concentration exhibited similar temporal trends and high correlation coefficient, it was underestimated by 19.1%. Given the reasonable performance of gas-phase chemistry and gas-particle partitioning, we attributed the discrepancies in SOA mass concentration and O:C and H:C possibly to the absence of particle-phase chemistry in the model. And the slight underestimation of gas-phase HOMs would not lead to higher O:C.

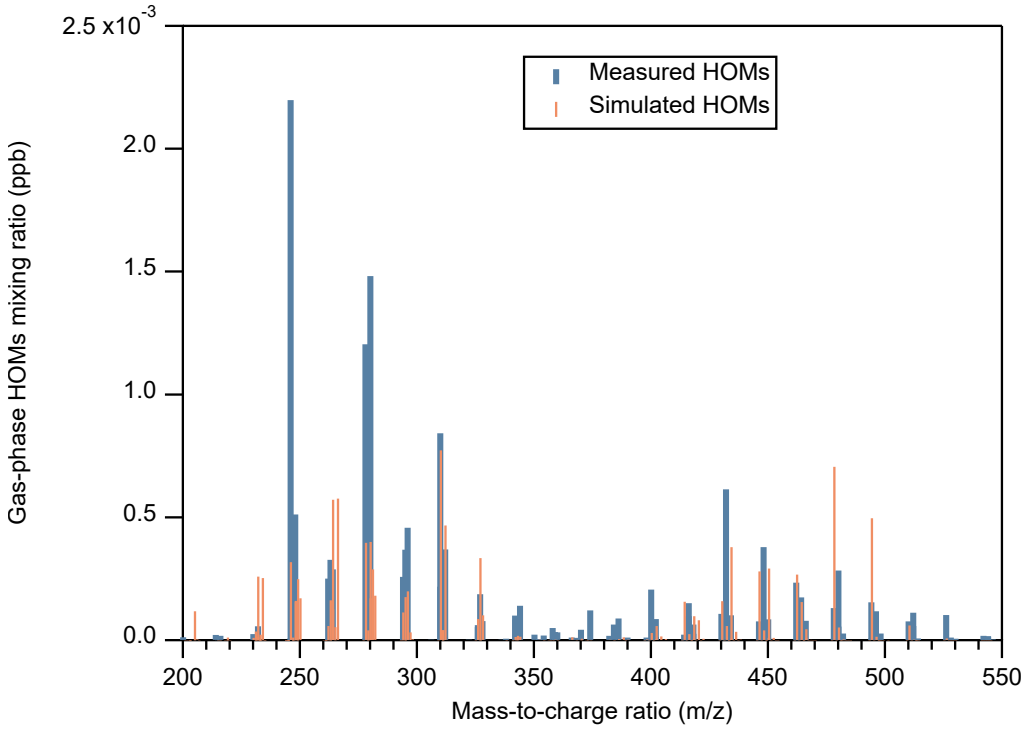

Fig. R8: Measured and simulated gas-phase HOMs mass spectra averaged over the first 5 min of experiment, during which gas-phase HOMs were rapidly accumulated and particle-phase concentrations were low.

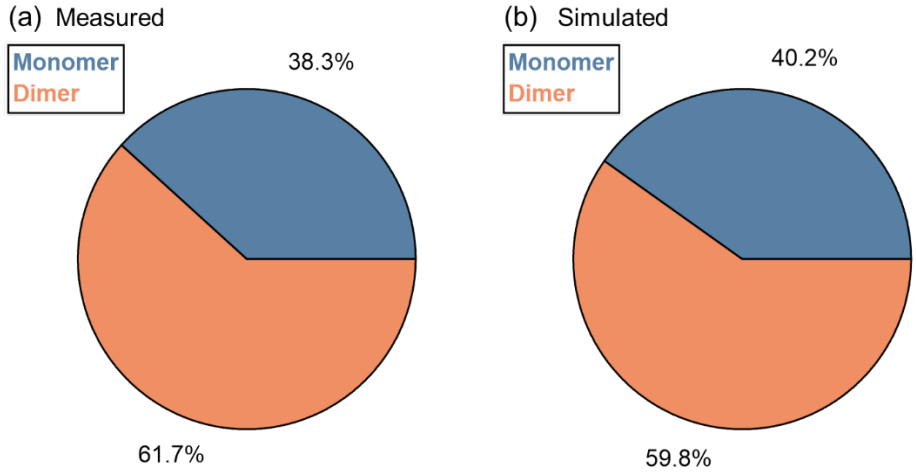

Fig. R9: Pie charts of (a) measured and (b) simulated gas-phase HOMs monomer and dimer fractions averaged over the first 5 min of the reaction.

In the revised manuscript, we have revised the discussion as follows (line 276-280).

"The gas-phase chemistry, including the loss of α-pinene (Fig. S7) and the composition of HOMs, is generally well reproduced (Fig. S9). The model reproduces the bimodal distributions of HOM monomers (m/z 230-380) and dimers (m/z 400-550), although the concentration of monomers is underestimated, especially below m/z 300. It also reasonably captures the fractions of HOM monomers and dimers (Fig. S10), while showing a slight underestimation of dimers in the simulation."

Figure S9-10 in the main text correspond to Fig. R8-9 here.

(9) It is difficult to observe the differences between the simulated and observed particle size distributions in Figure 5. It is recommended to supplement the figure with a two-dimensional curve showing the particle number concentration as a function of particle size at a specific time.

Response:

Accepted. The geometric mean diameter of SOA reflects only the general tendency of the size distribution and does not capture information about peak width. To address this limitation, we have added two-dimensional $dN/dlogD_p$ plots for reaction hours 2, 4, 6, and 8 (Fig. R10 below and Fig. S14 in the revised manuscript). These plots provide a more clear comparison and illustrate the differences between the simulated and observed size distributions (i.e., the simulated distributions are flatter and broader).

We have added the following text in the revised manuscript (line 377-379).

"Figure S15 presents the $dN/dlog_{10}D_p$ versus PSD at 2, 4, 6, and 8 h of reaction time, clearly illustrating that the simulated PSDs were broader and flatter than measurement."

The Fig. S15 in the main text corresponds to Fig. R10 here.

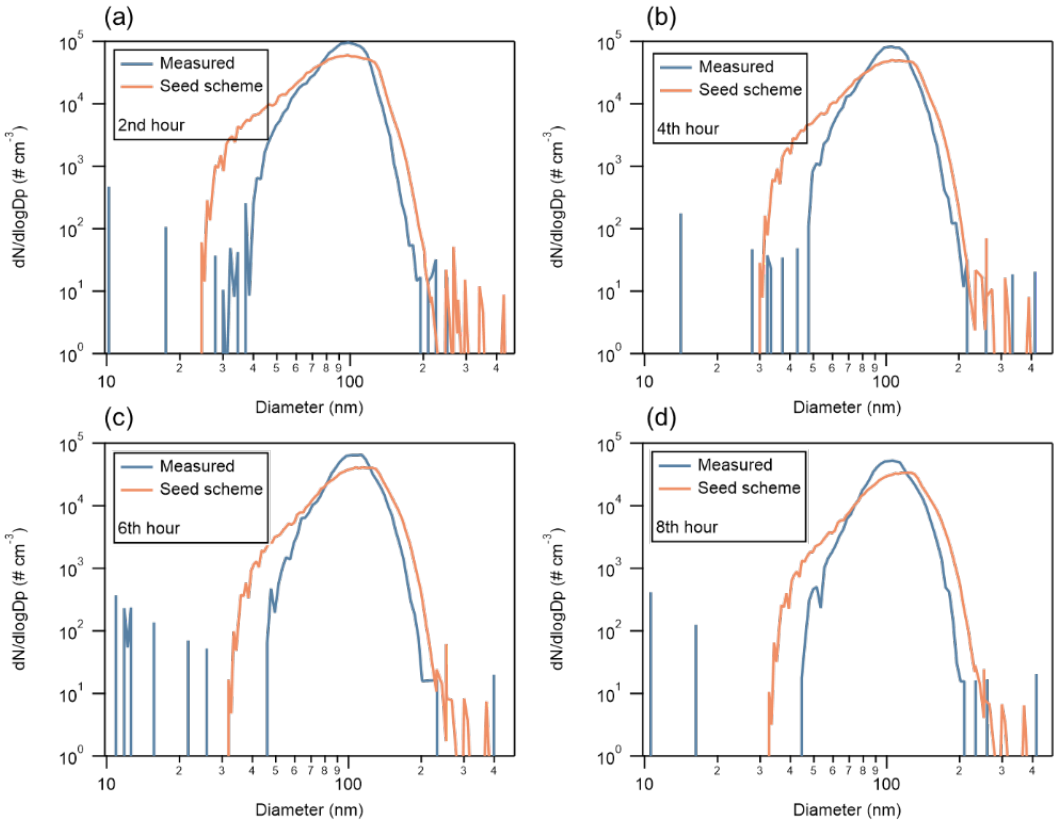

Fig. R10: (a-d) Number particle size distribution (dN/dlogDp) at reaction hours 2, 4, 6, and 8.

(10) How were the κ values in Figure 6 measured? This is not explained in the text. Furthermore, why does the measured κ value show a sudden decrease at the second hour, while the simulated value does not exhibit such a change? As shown in the figure, κ values differ under different SS conditions, so what SS was used to determine the simulated κ?

Response:

Accepted. As mentioned in the response to comment 4, we have added a detailed description of how κ is measured.

The sharp decrease in the measured κ around hour 2 occurs because the SS switched from 0.73% to 0.19%, leading to a much lower CCN number concentration and consequently affecting the inferred critical activation dry diameter (D_{crit}) and the resulting κ. After hour 2, κ values are showed only for SS = 0.19% and 0.37%, because the D_{crit} derived from fitting CCN/CN activation curves at SS = 0.73% and 0.55% have too large uncertainties as almost all particles are activated.

Since the measured κ values are derived directly from CCN number concentrations, they necessarily correspond to specific SS. The dependence of κ on SS may result from the dependence of chemical composition on particle size as the D_{crit} at different SS are different as we discussed in the manuscript (Zhao et al., 2015; Zhang et al., 2023). In contrast, the simulated κ values of bulk SOA are computed from the modeled SOA molecular composition, vapor pressure, density, dry diameter, temperature, and surface tension (Kreidenweis et al., 2005). As shown in Table S2, simulated chemical composition and κ of SOA did not show dependences on particle size in the size range of the D_{crit} measured at various SS. Therefore, simulated κ did not correspond to a specific SS.

In the revised manuscript, we have added the following text to clarify this problem (line 398-399).

"The sudden decrease in κ measured at ~2 h of reaction is attributed to the decrease of the set SS from 0.73% to 0.19%. In contrast, the simulated κ was formula-based and did not correspond to specific SS."

And line 410-411:

"After ~2 h, κ values were showed only for SS = 0.19% and 0.37%, because the D_{crit} derived from fitting CCN/CN activation fraction curves at SS = 0.73% and 0.55% had too large uncertainties as almost all particles were activated."

(11) When SS = 0.19%, the simulated CCN concentration is much higher than the measured value. The authors attribute this overestimation to the wider and flatter particle size distribution in the simulation. Why does this overly broad particle size distribution not cause significant deviations under other high SS conditions?

Response:

The procedure for calculating simulated CCN is as follows. Using the κ-Köhler equation, we first compute the critical activation dry diameter (D_{crit}) corresponding to each SS based on the simulated κ values. We then integrate the particle number size distribution above D_{crit} to obtain the CCN number concentration for each SS. Thus, the simulated CCN depends directly on both D_{crit} and the PSD.

As shown in the figure R11 below (Fig. S17 in the revised manuscript), we present the simulated and observed D_{crit} values for the four SS levels, along with their corresponding size distributions, before and after hour 2 of the experiment. For SS = 0.19% and 0.37%, the simulated κ values are overestimated, leading to underestimated D_{crit} (located to the left of the observed D_{crit}; panels (a) and (b)). Conversely, for SS = 0.55% and 0.73%, the simulated κ values are underestimated, yielding overestimated D_{crit} (to the right of the observations; panels (c) and (d)).

At SS = 0.19%, the combination of underestimated D_{crit} and the simulated size distribution being broader and flatter in peak height leads to a substantial overestimation of CCN. In contrast, for the other SS levels, despite the broader simulated size distributions, the simulated and observed D_{crit} values are very similar and lie to the left of the dN/dlogDp peak. As a result, the flatter and broader simulated size distributions tend to offset the effect of the D_{crit} differences, producing CCN number concentrations that deviate only slightly from the observations.

In the revised manuscript, we have revised the following text to clarify this problem (line 413-431).

"Figure S18 presents the PSD and D_{crit} at four SS levels corresponding to time points before and after 2 h, providing additional context for interpreting the discrepancies between simulated and measured CCN. At the higher SS levels of 0.73% and 0.55%, the simulated CCN number concentrations closely matched the measurements throughout the reaction (R^2 = 0.88-0.99), except for a more rapid increase during the initial period at SS = 0.73%. Although κ was underestimated at these SS, leading to slightly overestimated D_{crit}, the simulated and measured D_{crit} were still very similar and both positioned to the left of the PSD peak (Fig. S18c and d). Under these conditions, the broader and flatter simulated PSD introduced a compensating effect, resulting in simulated CCN concentrations that were very close to the measurements. The slight overestimation of CCN before 0.6 h at SS = 0.73% was primarily attributable to the low bias in simulated κ, since the simulated and measured PSD were identical during this period.

At SS = 0.37%, the simulated CCN number concentrations also agreed closely with measured CCN (R^2 = 0.98) with a mean bias of -3.9% ± 1.9%. This good agreement corresponds to the smallest discrepancy between simulated and measured κ at this SS. Although κ was slightly overestimated at SS = 0.37%, the simulated and measured D_{crit} remained very similar and both lay to the left of the PSD peak (Fig. S18b). As a result, the broader and flatter PSD did not introduce a noticeable bias in simulated CCN.

In contrast, at SS = 0.19%, the simulated CCN number concentrations were obviously overestimated by a factor

of >4 throughout the reaction. At this lowest SS, the required D_{crit} is largest, and both simulated and measured D_{crit} were located to the right of the PSD peak (Fig. S18a). The high bias in simulated κ at this SS further reduced the simulated D_{crit}, and this underestimation, combined with the broader and flatter simulated PSD, resulted in pronounced overprediction of CCN relative to the measurements."

Figure S18 in the main text corresponds to Fig. R11 here.

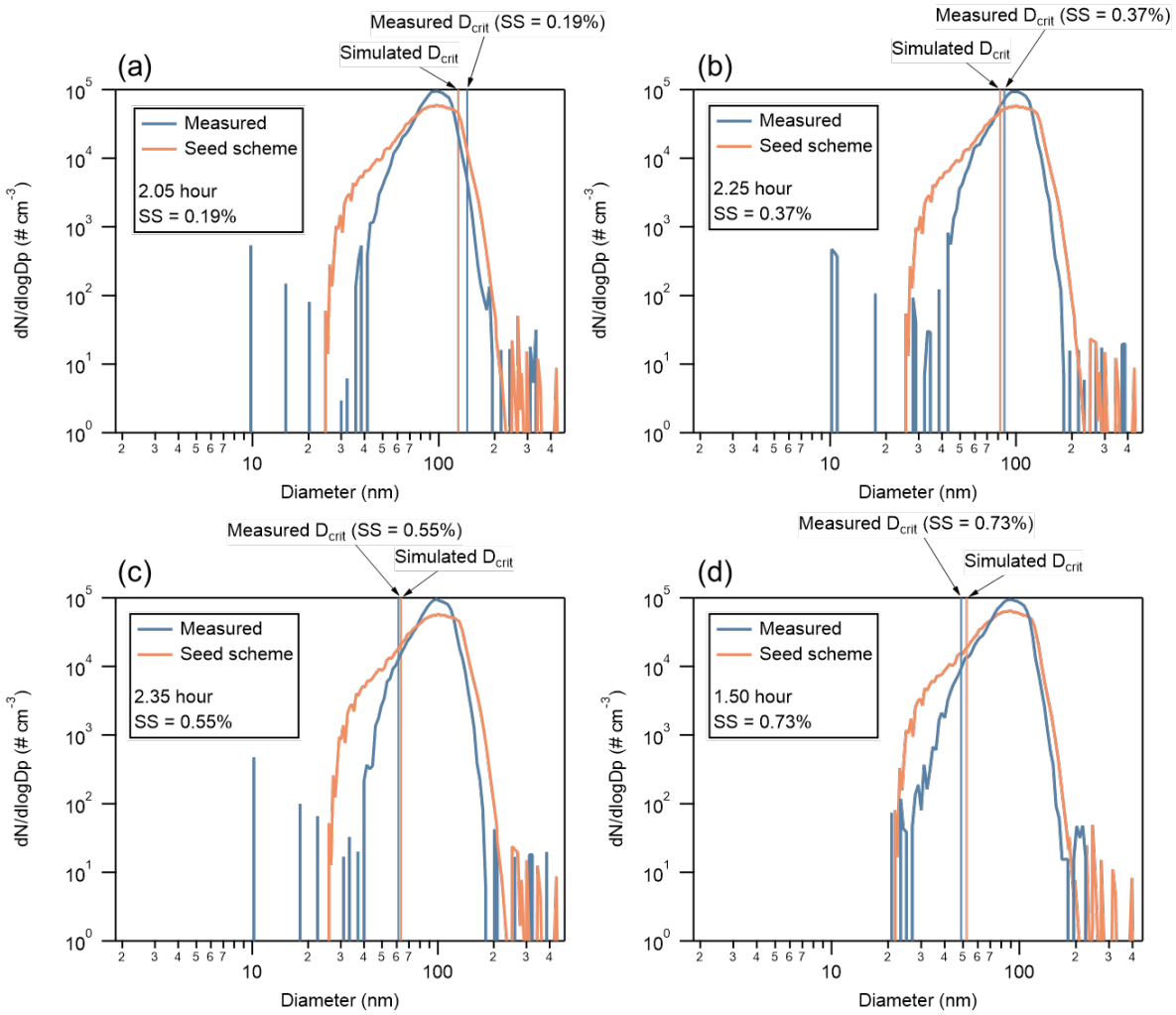

Fig. R11: (a-d) Measured and simulated number particle size distribution (dN/dlogDp) at four SS and corresponding measured or simulated critical activation dry diameter (D_{crit}).

In addition to the above revisions as our response to the reviewer, we have also polished the obscure and poorly expressed sentences in the revised manuscript.

Abstract in line 18-33:

"**Abstract.** Secondary organic aerosols (SOA) contribute significantly to cloud condensation nuclei (CCN), which depend on particle size distribution (PSD), chemical composition and the hygroscopicity parameter (κ). Simulating SOA and CCN in chemical transport models relies on parameterizations, which need to be evaluated and improved against process-level models as a benchmark. Here, we simulated SOA concentration, chemical composition, PSD, κ, and CCN in α-pinene ozonolysis, a classical system for SOA studies, using a process-level box model PyCHAM with near-explicit chemical mechanisms. We assessed how CCN, chemical composition, PSD and κ can be modelled against measurements and evaluated the influence of these factors on CCN simulation. The model well simulated SOA mass concentration but overestimated O:C and H:C ratios, suggesting a possible lack of particle-phase chemistry. Highly oxygenated molecules (HOMs) contributed substantially to SOA mass. Simulated κ closely agreed with measurements at moderate supersaturation (0.37%) but was overestimated at low supersaturation (0.19%) and underestimated at high supersaturation (0.55% and 0.73%). Particle growth and number concentrations were reasonably reproduced, though the simulated PSD was broader and flatter than measurement. Simulated CCN concentrations agreed well with measurements at moderate to high supersaturation (0.37–0.73%) but were overestimated at low supersaturation (0.19%). Sensitivity analysis highlights the importance of accurately representing both PSD and κ for reliable CCN prediction, especially at supersaturation < 0.4%. This study also highlights that HOM formation, finer PSD resolution and improved κ parameterizations are warranted in future chemical transport models, and evaluates the ability and limitations of this benchmark model."

References

Kreidenweis, S. M., Koehler, K., DeMott, P. J., Prenni, A. J., Carrico, C., and Ervens, B.: Water activity and activation diameters from hygroscopicity data - Part I: Theory and application to inorganic salts, Atmos. Chem. Phys., 5, 1357–1370, https://doi.org/10.5194/acp-5-1357-2005, 2005.

Moore, R., Nenes, A., and Medina, J.: Scanning Mobility CCN Analysis– A method for fast measurements of size resolved CCN distributions and activation kinetics, Aerosol Sci. Tech., 44, 861–871, DOI:10.1080/02786826.2010.498715, 2010.

O'Meara, S. P., Xu, S., Topping, D., Alfarra, M. R., Capes, G., Lowe, D., Shao, Y., and McFiggans, G.: PyCHAM (v2.1.1): a Python box model for simulating aerosol chambers, Geosci. Model Dev., 14, 675–702, https://doi.org/10.5194/gmd-14-675-2021, 2021.

Petters, M. D. and Kreidenweis, S. M.: A single parameter representation of hygroscopic growth and cloud condensation nucleus activity, Atmos. Chem. Phys., 7, 1961–1971, https://doi.org/10.5194/acp-7-1961-2007, 2007.

Roldin, P., Ehn, M., Kurtén, T. et al.: The role of highly oxygenated organic molecules in the Boreal aerosol-cloud-climate system, Nat Commun, 10, 4370, https://doi.org/10.1038/s41467-019-12338-8, 2019.

Zaveri, R., Easter, R., Fast, J., and Peters, L.: Model for Simulating Aerosol Interactions and Chemistry (MOSAIC), J. Geophys. Res., 113, D13204, https://doi.org/10.1029/2007JD008782, 2008.

Zhao, D. F., A. Buchholz, B. Kortner, P. Schlag, F. Rubach, A. Kiendler-Scharr, R. Tillmann, A. Wahner, J. M. Flores, Y. Rudich, et al.: Size-dependent hygroscopicity parameter (κ) and chemical composition of secondary organic cloud condensation nuclei, Geophys. Res. Lett., 42, 10,920–10,928, https://doi:10.1002/2015GL066497, 2015.

Zhao, D. F., Buchholz, A., Kortner, B., Schlag, P., Rubach, F., Fuchs, H., Kiendler-Scharr, A., Tillmann, R., Wahner, A., Watne, Å. K., Hallquist, M., Flores, J. M., Rudich, Y., Kristensen, K., Hansen, A. M. K., Glasius, M., Kourtchev, I., Kalberer, M., and Mentel, Th. F.: Cloud condensation nuclei activity, droplet growth kinetics, and hygroscopicity of biogenic and anthropogenic secondary organic aerosol (SOA), Atmos. Chem. Phys., 16, 1105–1121, https://doi.org/10.5194/acp-16-1105-2016, 2016.

Zhang, C., Guo, Y., Shen, H., Luo, H., Pullinen, I., Schmitt, S. H., et al.: Contrasting influence of nitrogen oxides on the cloud condensation nuclei activity of monoterpene-derived secondary organic aerosol in daytime and nighttime oxidation, Geophys. Res. Lett., 50, e2022GL102110, https://doi.org/10.1029/2022GL102110, 2023.